

Dynamic optimal power flow of active distribution network based on LSOCR and its application scenarios

Weiqli Meng¹, Dongran Song¹, Xiaofei Deng^{2,*}, Mi Dong¹, Jian Yang¹, Rizk M. Rizk-Allah^{3,4}, Václav Snášel⁴

¹ School of Automation, Central South University, Changsha, 410083, China; mengweiqli@csu.edu.cn, humble_szy@163.com, mi.dong@csu.edu.cn, jian.yang@csu.edu.cn

² School of Information Technology and Management, Hunan University of Finance and Economics, Changsha, 410205, China; xiaofei0228@163.com

³ Department of Basic Engineering Science, Faculty of Engineering, Menoufia University, Shebin El-Komm 32511, and Scientific Research Group in Egypt (SRGE), Egypt; rizk_masoud@yahoo.com

⁴ Faculty of Electrical Engineering and Computer Science, VŠB-Technical University of Ostrava, 70800 Pruba-Ostrava, Czech Republic; vaclav.snasel@vsb.cz

* Correspondence: xiaofei0228@163.com; Tel.: 13974341334

Abstract: Optimal power flow (OPF) is a crucial aspect of distribution network planning and operation. Conventional heuristic algorithms fail to meet the system requirements for speed and accuracy, while linearized OPF approaches are inadequate for distribution networks with high R/X ratios. To address these issues and cater to multi-period scenarios, this study proposes a dynamic linearized second-order cone programming-based (SOCP) OPF model. The model is built by first establishing a dynamic OPF model based on linearized second-order conic relaxation (LSOCR-DOPF). The components of the active distribution network, such as renewable energy power generation units, energy storage units, on-load-tap-changers, static var compensators, and capacitor banks, are then modeled separately. The model is implemented in MATLAB and solved by YALMIP and GUROBI. Finally, three representative scenarios are used to evaluate the model accuracy and effectiveness.

Keywords: optimal power flow (OPF); active distribution network; linearized second-order conic relaxation (LSOCR); network reconfiguration; ZIP load

1. Introduction

Access to various distributed energy resources (DERs) brings new challenges to the planning and operation of the distribution network [1–3]. Recently, researchers have shown an increased interest in the active distribution network. It is particularly urgent to develop optimization algorithms and high-performance computing tools applicable to various fields of active distribution networks. Ref. [4] pointed out that there are three kinds of optimization problems of the active distribution network: optimal power flow (OPF), unit commitment, and operation planning. Their essence is distribution network optimization, while having different optimization scale. The OPF is of great significance in the development process of the distribution network and is the most common and fundamental optimization problem in power systems [5]. The research on distribution network OPF mainly focuses on the alternating current power flow (AC-OPF). Exploring a solution method to enhance the solution speed of distribution network AC-OPF while ensuring its optimal operation and fulfilling the requirements of active distribution network planning and operation has been a major concern in the field of power system research. As a non-convex optimization problem, the OPF is difficult to solve. It is easy to fall into local optimum in the process of solving and is proved to be an NP-hard problem [6,7]. The power flow constraints are characterized by nonlinearity, and hence the essence

Citation: To be added by editorial staff during production.

Academic Editor: Firstname Last-name

Received: date

Revised: date

Accepted: date

Published: date



Copyright: © 2023 by the authors. Submitted for possible open access publication under the terms and conditions of the Creative Commons Attribution (CC BY) license (<https://creativecommons.org/licenses/by/4.0/>).

of OPF lies in nonlinear programming. The methods for solving OPF problems can be broadly categorized into the following three categories:

1) Pursuit of local optimal solutions, including early classical methods [8] (such as Simplified Gradient Method, Newton Method, Sequential Quadratic Programming, Interior Point Method) and recent rapidly-developing heuristic algorithms [4];

2) Approximation of power flow equality constraints. For example, the AC-OPF constraints can be approximately linearized as direct current power flow constraints, and the resultant direct current optimal power flow (DC-OPF) problem can be solved accordingly [9];

3) Relaxation of the power flow equality constraint using convex relaxation techniques [10].

The methods of seeking local optimal solutions, due to their advantages such as simplicity and ease in simulating complex constraints, have been widely applied in solving nonlinear programming models [11]. However, due to the non-convex nature of the OPF problem, these methods cannot guarantee the quality of the solution, and it is impossible to measure the gap between the locally optimal solution and the globally optimal solution. The methods that approximate the power flow equation constraints, such as the DC-OPF, present several obvious drawbacks. Firstly, they can be challenging to apply to research areas related to voltage and reactive power, as well as distribution networks with high R/X ratios. Secondly, the optimal solution of the DC-OPF problem may not be a feasible solution of the original OPF problem, leading to the need for constant adjustment of the tightness of DC-OPF constraints and the need to solve again during the actual optimization process [12]. With the numerous issues associated with seeking local optima and approximating the current flow equality constraints, it requires new methods to deal with the current flow equality constraints.

The convex relaxation technique has gained significant attentions in recent years due to its advantages and potential in solving OPF problems in the field of power system optimization. The use of convex relaxation techniques, particularly Second-order cone programming (SOCP) relaxation, is increasingly prevalent. The SOCP mainly converts the original model into a convex programming form, thus obtaining the globally optimal solution and a good computational speed. Refs. [13,14] systematically established a branch flow model (BFM) based on Distflow [15] to solve the OPF model framework, and presented two relaxation steps: 1) Elimination of voltage and current phase angles; 2) Second Order Conic Relaxation (SOCR). The authors also demonstrated the relaxation accuracy of SOCR. As a typical representative of SOCP, SOCR can be summarized in the mathematical field as the classic "dimensionality relaxation-return mapping" process: A new variable is introduced to elevate the dimensionality of the original problem; then, in the elevated problem, non-convex constraints are relaxed and a solution is obtained; finally, the solution of the original problem is recovered through a return mapping.

The main challenge in using SOCR to solve the optimal power flow lies in accurately satisfying the conditions of the relaxed model. Refs. [16,17] provided a comprehensive summary of the sufficient conditions for the accuracy of SOCR under radiated network conditions, which are divided into three categories: power injection constraints, voltage amplitude constraints, and node voltage phase angle deviations, and corresponding explanations are given for the optimal power flow objective function. After the examination of Ref. [17], further research on the exact relaxation sufficient condition has been extensively conducted. Ref. [18] expanded upon the sufficient conditions for the accuracy of SOCR in the presence of high penetration of distributed generation. Refs. [19,20] highlighted the shortcomings of the second sufficient condition in Ref. [17] as it neglected the impact of the grounding branch power flow on line capacity, and proposed an improved sufficient condition. Additionally, Refs. [21,22] conducted a thorough and precise approximation proof of the polyhedral solid approximation method in second-order cone programming, enabling the direct linearization of equivalent SOCR and improving the efficiency of solution models while maintaining optimal solution quality. Refs. [23-25]

extended the constant power load model to a comprehensive load model under a rectangular coordinate system and applied it to the solution of the OPF. In addition, in the active distribution network planning and operation optimization model, discrete variables will inevitably appear, which turns the original problem into a mixed integer linear programming (MILP) [24]. With the continuous development and maturity, commercial optimization software (GUROBI, CPLEX, MOSEK, etc.) has been widely used in distribution network reconstruction [26], reactive power optimization [27], distribution network planning [11,28], etc.

It is noteworthy that, the above studies are mostly limited to the traditional single-period static OPF category, while the actual optimization requires the overall coordination of multi-period, which is actually a dynamic optimal power flow (DOPF). Meanwhile, traditional second-order cone programming is not suitable for fast solutions in large-scale power systems of the future. Most of the existing distribution network models only include power generation units and energy storage devices, and rarely consider reactive power compensation devices and other active management devices at the same time [29]. Additionally, compared to the rectangular coordinate system, the current form in polar coordinates is more common.

Therefore, In order to meet the operational requirements of multi-period scenarios, various complex constraints, and fast large-scale solutions for active distribution networks, this paper proposes a linearized second-order cone relaxation dynamic optimal power flow (LSOCR-DOPF) model of the distribution network and explores the linear modeling method of key constraints of active distribution network participating elements (such as on-load-tap-changer (OLTC), static var compensator (SVC), capacitor banks (CB), the energy storage system (ESS), etc.). The nonlinear OPF problem of the distribution network is transformed into a computationally efficient solution utilizing MILP, with a comprehensive explanation of the network's constraints on radiation and connectivity. On this basis, this paper further presents an innovative approximation of the ZIP load model under polar coordinates, and validates the effectiveness of the OPF framework through three scenarios: power coordination optimization, network reconfiguration, and ZIP load application. The main contributions of this study can be summarized as follows:

- Present the LSOCR-DOPF model, which is based on branch power flow analysis, for the active distribution network.
- Explore the linear modeling method for the constraints of various active management units, including OLTC, SVC, CB, ESS, etc.
- Validate the LSOCR-DOPF model through simulation experiments in three typical scenarios, power coordination optimization, network reconfiguration, and ZIP load application.

The article is organized as follows: The second section presents the LSOCR-DOPF model for active distribution networks and the design of various active management units based on branch power flow analysis. The third section discusses the results of three simulation experiments and provides a comprehensive analysis and discussion of the findings. Finally, the fourth section presents the conclusion and future perspectives.

2 Methodology

2.1 LSOCR-DOPF model of the distribution network

2.1.1 Basic structure of distribution network

In most distribution networks, the steady-state power operation mode is radial and its structure is depicted in Figure 1. For radial topology network, the node directed graph can be used for equivalent analysis, assuming that branch ij represents the positive direction of flow direction from node i to node j . $\delta(j)$ is the collection of branch end nodes with j as the head node, and $\pi(j)$ is the collection of branch end nodes with j as the end node. Besides, S_{ij} and S_i represents complex power, $S_{ij} = P_{ij} + Q_{ij}i$ and $S_i = p_i + q_i i$.

And branch complex impedance $Z_{ij} = r_{ij} + x_{ij}i$; Set B represents the set of all nodes in the network; In the traditional OPF, the voltage remains constant. If OLTC is installed, the voltage will change with the OLTC transformation ratio; E represents the collection of all branches in the network. There are N^{sub} substations, N^{bus} nodes and N^{Line} line branches in the network.

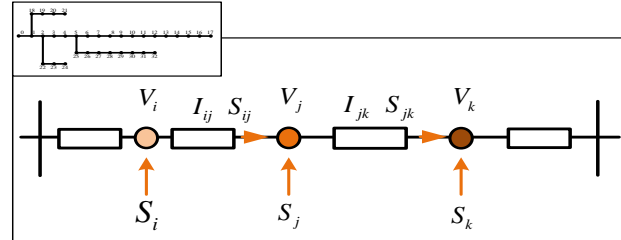


Figure 1. Structure of radial distribution network.

2.1.2 Basic OPF model based on BFM

Generally, the basic model of optimal power flow based on branch power flow (BFM-OPF) is expressed as follows [14]:

$$\min f(p, q, P, Q, V, I) \quad (1)$$

$$\text{s.t.} \begin{cases} p_j = \sum_{k \in \delta(j)} P_{jk} - \sum_{i \in \pi(j)} (P_{ij} - I_{ij}^2 r_{ij}) + g_j V_j^2, \forall j \in B \\ q_j = \sum_{k \in \delta(j)} Q_{jk} - \sum_{i \in \pi(j)} (Q_{ij} - I_{ij}^2 x_{ij}) + b_j V_j^2, \forall j \in B \end{cases} \quad (2)$$

$$V_j^2 = V_i^2 - 2(P_{ij} r_{ij} + Q_{ij} x_{ij}) + I_{ij}^2 (r_{ij}^2 + x_{ij}^2), \forall ij \in E \quad (3)$$

$$I_{ij}^2 = \frac{P_{ij}^2 + Q_{ij}^2}{V_i^2}, \forall ij \in E \quad (4)$$

$$I_{-ij} \leq I_{ij} \leq \bar{I}_{ij}, \forall ij \in E \quad (5)$$

$$V_{-j} \leq V_j \leq \bar{V}_j, \forall j \in B \quad (6)$$

$$\begin{cases} p_j \in R_j^p \\ q_j \in R_j^q \end{cases}, \forall j \in B \quad (7)$$

where, p_j and q_j represent the active and reactive power injections, respectively, at each node; P_{ij} and Q_{ij} denote the active and reactive current flow in each branch; r_{ij} and x_{ij} correspond to the resistance and reactance of each branch, individually; g_j and b_j are the ground conductance and ground susceptance of node j , separately; B and E refer to the node and branch sets, specifically, in the power distribution network.

From equations (1) to (7), it can be inferred that: 1) The optimization variables for OPF consist of node injection power (p, q), branch power flow (P, Q), node voltage (V), and branch current (I), with the substation node voltage not considered as an optimization variable; 2) Equation (1) represents the objective function, which can be the minimization of network losses and substation node power purchases; 3) Equations (2) to (6) embody the general constraints that are common to most radial networks, including balance constraints and security constraints for power flow; 4) Equation (7) introduces node-dependent constraints that are subject to change based on the employed model.

2.1.3 Multi-period LSOCR-OPF model

In order to convert power flow constraints into quadratic cone constraints, additional variables of cone optimization need to be set:

$$\begin{cases} \bar{I}_{ij} = I_{ij}^2 \\ \bar{V}_{ij} = V_{ij}^2 \end{cases} \quad (8)$$

Substitute equation (8) into equations (2) ~ (6) to change the power flow constraint as follows:

$$\min f(p, q, P, Q, V, I) \quad (9)$$

$$\text{s.t.} \begin{cases} p_j = \sum_{k \in \delta(j)} P_{jk} - \sum_{i \in \pi(j)} \left(P_{ij} - \bar{I}_{ij} r_{ij} \right) + g_j \bar{V}_j, \forall j \in B \\ q_j = \sum_{k \in \delta(j)} Q_{jk} - \sum_{i \in \pi(j)} \left(Q_{ij} - \bar{I}_{ij} x_{ij} \right) + b_j \bar{V}_j, \forall j \in B \end{cases} \quad (10)$$

$$\bar{V}_j = \bar{V}_i - 2 \left(P_{ij} r_{ij} + Q_{ij} x_{ij} \right) + \bar{I}_{ij} \left(r_{ij}^2 + x_{ij}^2 \right), \forall ij \in E \quad (11)$$

$$\left\| \begin{matrix} 2P_{ij} \\ 2Q_{ij} \\ \bar{I}_{ij} - \bar{V}_j \end{matrix} \right\|_2 \leq \bar{I}_{ij} + \bar{V}_j, \forall ij \in E \quad (12)$$

$$I_{-ij}^2 \leq \bar{I}_{ij} \leq \bar{I}_{ij}^{-2}, \forall ij \in E \quad (13)$$

$$V_{-j}^2 \leq \bar{V}_j \leq \bar{V}_j^{-2}, \forall j \in B \quad (14)$$

With this, the SOCR-OPF (a typical Mixed-Integer Second Order Cone Programming, MISOCP) model is fully modeled. Among them, the second-order cone programming represented by equation (12) can be described as:

$$\frac{P_{ij}^2 + Q_{ij}^2}{\bar{V}_j} \leq \bar{I}_{ij}, \forall ij \in E \quad (15)$$

The equation (15) can be uniformly expressed as:

$$\sqrt{x_1^2 + x_2^2} \leq x_3; x_1 = P_{ij}, x_2 = Q_{ij}, x_3 = \sqrt{\bar{V}_j \bar{I}_{ij}} \quad (16)$$

So far, the power flow constraint has been transformed from a nonlinear programming model to a quadratic cone programming model composed of equations (9) ~ (14). The polyhedron approximation method proposed in Refs. [21,22] is used to linearize equation (16), so that the MISOCP model can be approximately converted into a MILP model for solution. The approximate expression of the polyhedron of the three-dimensional SOCR constraint (16) is:

$$\begin{cases} a_0 \geq |x_1|; b_0 \geq |x_2|; a_k = a_{k-1} \cos \frac{\pi}{2^{k+1}} + b_{k-1} \sin \frac{\pi}{2^{k+1}} \\ b_k \geq \left| -a_{k-1} \sin \frac{\pi}{2^{k+1}} + b_{k-1} \cos \frac{\pi}{2^{k+1}} \right|, k = 1, 2, \dots, K \\ a_K \leq x_3; b_K \leq a_K \tan \frac{\pi}{2^{k+1}} \end{cases} \quad (17)$$

where, K represents the number of facets in a polyhedron. a_0 and b_k are auxiliary variables.

The other types can be simplified by utilizing the equation $a_k = a_{k-1} \cos(\pi/2^{k+1}) + b_{k-1} \sin(\pi/2^{k+1})$, thereby eliminating K equality constraints and K variables (a_k). The other types can be simplified using a_k to eliminate K equality constraints and K variables. The error term [21] of the polyhedral approximations of the three-dimensional second-order cone constraint is:

$$\sqrt{x_1^2 + x_2^2} \leq \left[1 + \frac{1}{\cos\left(\frac{\pi}{2^{K+1}}\right)} \right] x_3 \quad (18)$$

According to Equation (18), when $K=11$, the error is about 6×10^{-7} . Therefore, the MISOCP model for active distribution network reconfiguration is approximately equivalent to the MILP model. At this point, the improved version of SOCR-OPF, namely the LSOCR-OPF model, is fully modeled.

The previously described model represents the conventional single-period OPF model. However, since most practical applications involve multi-period optimization, this study converts the single-period (static) power flow model into a multi-period (dynamic) OPF model. For clarity of expression, the following dynamic OPF model, based on LSOCR, can be expressed in vector form:

$$\begin{cases} \min & \sum_{t \in T} f(x_t) \\ \text{s.t.} & x_t \in X_t, \forall t \\ & A_{ij,t} x_t \leq b_{ij,t}^T x_t, \forall t, \forall ij \in E \\ & \sum_{t \in T} B_t x_t \leq c \\ & \sum_{t \in T} C_t x_t = d \end{cases} \quad (19)$$

where, t is the period identification, T is the total number of time periods. $x_t \in X_t, \forall t$ represents the constraint relationship in the traditional single-period OPF model, such as upper and lower limit constraints, power flow equation constraints, etc. $\sum_{t \in T} B_t x_t \leq c$ is the second-order cone constraint relationship under each branch at each time.

Equation (19) adds the linear coupling relationship between multi-period periods to the objective function and constraint conditions. Some elements will be described in detail in the next section, such as OLTC, CB, ESS, etc. Hence, the further improved version of LSOCR-OPF, namely LSOCR-DOPF model, is fully modeled.

In order to facilitate understanding, additional explanation is required for the entire model transformation process (from AC-OPF to LSOCR-DOPF): Equations (8) and (16) respectively embody the phase angle relaxation and second-order cone relaxation of LSOCR-DOPF, and Figure 2 depicts the schematic diagram of the two-step relaxation process. The non-convex feasible region C_{AC-OPF} of the original AC-OPF problem will be relaxed into a convex second-order cone feasible region C_{OPF-cr} after phase angle relaxation and second-order cone relaxation. Then, the convex feasible region of the second-order cone is further linearized into the convex feasible region $C_{OPF-linear}$ of the integer programming by the polyhedral approximations. At this time, the optimal power flow problem in the original formulation has already been transformed into a convex optimization problem. Numerous studies, as demonstrated in Refs. [13,14,16,17], have substantiated the strict accuracy of the second-order cone relaxation (SOCR) approach for most distribution network structures, when the objective function is both a convex and strictly increasing function.

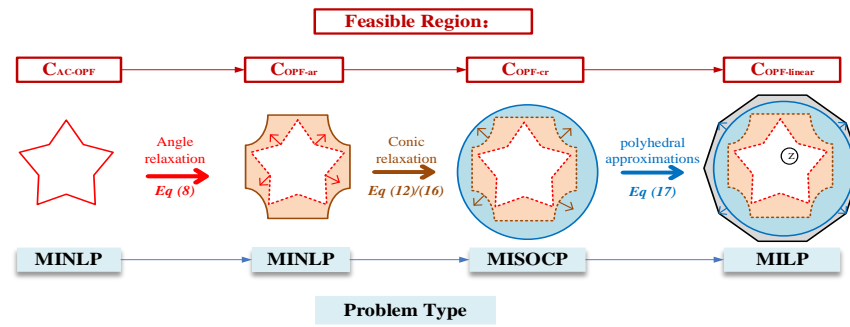


Figure 2. Proposed LSOCR for solving AC-OPF.

2.2 Active distribution network modeling

In this section, the active management components of the active distribution network are considered, including: ① Reactive compensation device (SVC and CB); ② Active power regulation device (Energy storage system and Electric vehicle mobile energy storage system); ③ on-load tap changer (OLTC); ④ Distributed generation power regulation. Given that the objective function in the OPF is either linear or quadratic, the quadratic form can be effectively addressed by means of piecewise linearization. This paper linearizes the constraints related to the active management equipment. Given that the network reconfiguration is of great significance for active distribution network planning and optimal operation [30], this paper discusses the constraints related to grid reconfiguration, such as radial constraints. In addition, in order to ensure the applicability of the model, this paper further considers the ZIP load.

2.2.1 Active distribution network units modeling

1. Active power regulation device

(1) Modeling of discrete reactive power compensation (CB).

$$\begin{cases} Q_{j,t}^{\text{CB}} = y_{j,t}^{\text{CB}} Q_j^{\text{CB,step}} \\ y_{j,t}^{\text{CB}} \leq Y_j^{\text{CB,m}} \end{cases}, \forall t, \forall j \in B^{\text{CB}} \quad (20)$$

where, B^{CB} is the set of CB nodes; $y_{j,t}^{\text{CB}}$ is the number of groups put into operation and the discrete variable value; $Y_j^{\text{CB,max}}$ is the upper limit of the number of CB groups connected by node j ; $Q_j^{\text{CB,step}}$ is the compensation power of each group of CB. Considering factors such as equipment life or economy, discrete reactive compensation is mostly limited by the number of adjustments, so it generally includes the total number of operations in multiple periods; $N_j^{\text{CB,max}}$ is the upper limit of operation times:

$$\sum_{t \in T} |y_{j,t}^{\text{CB}} - y_{j,t-1}^{\text{CB}}| \leq N_j^{\text{CB,m}}, \forall t, \forall j \in B^{\text{CB}} \quad (21)$$

In addition, for the absolute value constraint in the above equation, add an auxiliary variable $\delta_{j,t}^{\text{CB}} = |y_{j,t}^{\text{CB}} - y_{j,t-1}^{\text{CB}}|$ that represents the change of CB compensation capacity between adjacent periods, corresponding to:

$$\begin{cases} \sum_{t \in T} \delta_{j,t}^{\text{CB}} \leq N_j^{\text{CB,m}} \\ -\delta_{j,t}^{\text{CB}} Y_j^{\text{CB,m}} \leq y_{j,t}^{\text{CB}} - y_{j,t-1}^{\text{CB}} \leq \delta_{j,t}^{\text{CB}} Y_j^{\text{CB,m}} \end{cases}, \forall t, \forall j \in B^{\text{CB}} \quad (22)$$

(2) Modeling of continuous reactive power regulation device (SVC).

$$Q_j^{\text{SVC,min}} \leq Q_{j,t}^{\text{SVC}} \leq Q_j^{\text{SVC,m}}, \forall t, \forall j \in B^{\text{SVC}} \quad (23)$$

where, B^{SVC} is the node set containing SVC; $Q_j^{SVC, \min}$ and $Q_j^{SVC, \max}$ are the lower limit and upper limit of SVC compensation power respectively. Considering that in the process of active distribution network operation, with the increasing penetration of Distributed generation (DG) such as photovoltaic power generation, the system power flow may be reversed and overvoltage problems may occur, the lower limit Q of SVC compensation in this paper: $Q_j^{SVC, \min} < 0$.

2. OLTC model

The OLTC is used to adjust the voltage value at the low-voltage side of the bus node. Therefore, the substation bus node V_0 is further converted to the adjustable variable:

$$\begin{cases} V_j^2 \leq (V_{j,t}^{Base})^2, r_{j,t} \leq \bar{V}_j^2, \forall t, \forall j \in B^{OLTC} \\ r_j^{\min} \leq r_{j,t} \leq r_j^{\max} \end{cases} \quad (24)$$

where, B^{OLTC} refers to the node set of substation containing OLTC; $V_{j,t}^{Base}$ is the voltage value at the high voltage side of the transformer, which is a constant value; r_j^{\max} and r_j^{\min} are the square of the upper and lower limit of the OLTC adjustable transformation ratio; $r_{j,t}$ is the square of OLTC transformation ratio, defined as the ratio of the secondary side to the primary side, which is actually a discrete value variable, and can be further treated as the following relationship including 0-1 variables:

$$r_{j,t} = r_j^{\min} + \sum_s r_{j,s} \sigma_{j,s,t}^{OLTC}, \forall t, \forall j \in B^{OLTC} \quad (25)$$

where, $r_{j,s}$ represents the difference between OLTC gear s and the square of gear $s-1$, which is the adjacent adjustment increment. $\sigma_{j,s,t}^{OLTC}$ is a 0-1 identification variable. If it is considered to be constrained by the limit of adjustment times in practice, it can be further constrained as:

$$OLTC \begin{cases} \sigma_{j,1,t}^{OLTC} \geq \sigma_{j,2,t}^{OLTC} \geq \sigma_{j,SR_j,t}^{OLTC} \\ \delta_{j,t}^{OLTC,IN} + \delta_{j,t}^{OLTC,DE} \leq 1 \\ \sum_s \sigma_{j,s,t}^{OLTC} - \sum_s \sigma_{j,s,t-1}^{OLTC} \geq \delta_{j,t}^{OLTC,IN} - \delta_{j,t}^{OLTC,DE} SR_j, \forall t, \forall j \in B^{OLTC} \\ \sum_s \sigma_{j,s,t}^{OLTC} - \sum_s \sigma_{j,s,t-1}^{OLTC} \leq \delta_{j,t}^{OLTC,IN} SR_j - \delta_{j,t}^{OLTC,DE} \\ \sum_{t \in T} (\delta_{j,t}^{OLTC,N} + \delta_{j,t}^{OLTC,DE}) \leq N_j^{OLTC, \max} \end{cases} \quad (26)$$

where, $\delta_{j,t}^{OLTC,N}$ and $\delta_{j,t}^{OLTC,DE}$ represent OLTC gear adjustment change sign, which is 0-1 variable, if $\delta_{j,t}^{OLTC,IN} = 1$, then the gear value of OLTC at time $t-1$ is greater than the gear value at time t , $\delta_{j,t}^{OLTC,DE}$ is similar; SR_j^{OLTC} is the maximum range of gear change; $N_j^{OLTC, \max}$ is the maximum allowable adjustment times of OLTC gear at time T .

3. ESS model

In this part, the modeling of the energy storage system takes into account multiple-period constraints, including restrictions on its charging and discharging status, charging and discharging power, as well as capacity limitations.

(1) Power limit.

$$\begin{cases} u_{j,t}^{discharge} P_j^{discharge, \min} \leq P_{j,t}^{discharge} \leq u_{j,t}^{discharge} P_j^{discharge, \max} \\ u_{j,t}^{charge} P_j^{charge, \min} \leq P_{j,t}^{charge} \leq u_{j,t}^{charge} P_j^{charge, \max} \end{cases}, \forall t, \forall j \in B^{ESS} \quad (27)$$

(2) Charge and discharge status limit.

$$u_{j,t}^{discharge} + u_{j,t}^{charge} \leq 1, \forall j \in B^{ESS}, \forall t \quad (28)$$

(3) Capacity constraints.

$$\begin{cases} E_{j,t+1}^{\text{ESS}} = E_{j,t}^{\text{ESS}} + \alpha_j^{\text{charge}} P_{j,t}^{\text{charge}} - \alpha_j^{\text{discharge}} P_{j,t}^{\text{discharge}} \\ E_j^{\text{ESS,min}} \leq E_{j,t}^{\text{ESS}} \leq E_j^{\text{ESS,max}} \end{cases}, \forall j \in B^{\text{ESS}}, \forall t \quad (29)$$

where, B^{ESS} is the node set containing ESS; Equation (23) indicates that the ESS cannot be charged and discharged simultaneously at the same time, $u_{j,t}^{\text{charge}}$ and $u_{j,t}^{\text{discharge}}$ is $P_j^{\text{charge,min}}$ and $P_j^{\text{discharge,min}}$ are the upper and lower limits of ESS charging and discharging power respectively; $E_{j,t}^{\text{ESS}}$ is the power of the t period of ESS, $E_j^{\text{ESS,max}}$ and $E_j^{\text{ESS,min}}$ is the upper and lower limit value considering factors such as ESS life; α_j^{charge} and $\alpha_j^{\text{discharge}}$ is respectively the charge and discharge efficiency coefficient, generally $0 < \alpha_j^{\text{charge}} < 1$, $\alpha_j^{\text{discharge}} > 1$.

As a novel active management technique, electric vehicles can be considered as mobile active power energy storage systems [31]. Their basic model is largely similar to that of Energy Storage Systems (ESS). The equivalent injection power at each bus node in the distribution network can be represented as the clustering outcomes of individual electric vehicles.

4. Distributed generation model

Respectively modeling DG with or without reactive power:

(1) DG modeling without considering reactive power.

Currently, the modeling form of active management for DG primarily takes into account the possibility of DG allowing power shedding under certain conditions, and assumes that DG is only related to active power output [32], that is:

$$0 \leq P_{j,t}^{\text{DG}} \leq P_{j,t}^{\text{DG,PRE}}, \forall t, \forall j \in B^{\text{DG}} \quad (30)$$

where, B^{DG} is the node set containing DG; $P_{j,t}^{\text{DG,PRE}}$ is the predicted active power output of node j at time t .

(2) DG modeling considering reactive power.

With the maturity of active power regulation as a primary method in the study of DG and the advent of new technology, some DGs can have a certain impact on reactive power in the power grid, including outputting and absorbing reactive power. As a result, active management research focusing on reactive power of DG has emerged, mainly divided into constant power factor control and variable power factor control.

① Constant power factor control

$$\begin{cases} 0 \leq P_{j,t}^{\text{DG}} \leq P_{j,t}^{\text{DG,PRE}} \\ Q_{j,t}^{\text{DG}} = F_j^{\text{DG}} P_{j,t}^{\text{DG}} \end{cases}, \forall t, \forall j \in B^{\text{DG}} \quad (31)$$

② Variable power factor control

$$\begin{cases} 0 \leq P_{j,t}^{\text{DG}} \leq P_{j,t}^{\text{DG,PRE}} \\ Q_{j,t}^{\text{DG}} = F_{j,t}^{\text{DG}} P_{j,t}^{\text{DG}} \\ F_j^{\text{DG,min}} \leq F_{j,t}^{\text{DG}} \leq F_j^{\text{DG,max}}, \forall t, \forall j \in B^{\text{DG}} \\ Q_j^{\text{DG,min}} \leq Q_{j,t}^{\text{DG}} \leq Q_j^{\text{DG,max}} \end{cases} \quad (32)$$

where, $F_j^{\text{DG,max}}$ and $F_j^{\text{DG,min}}$ are the upper and lower limit of DG transformation ratio adjustment; $F_{j,t}^{\text{DG}}$ represents the ratio of reactive power to active power, and its optimization range can be converted from the power factor control range. At present, most of the literature will limit the reactive power $Q_j^{\text{DG,min}}$ and $Q_j^{\text{DG,max}}$ is set as a constant [24].

2.2.2 Radial constraints

Network reconfiguration is of great significance for the active distribution network with high renewable energy penetration, and radiation and islanding constraints are more important constraints in the process of optimal operation of the distribution network. Since the BFM model assumes the positive direction of the power flow, that is, $P_{ij} > 0$ indicates that the current flows from i to j , if $P_{ij} < 0$, the current direction is opposite; And, suppose σ_{ij} (0-1 variable) represents the state of branch ij , if $\sigma_{ij,t} = 0$, then the branch ij switch is open, and vice versa. It can be obtained in the same way in the distribution network planning, if $\sigma_{ij,t} = 1$, then the candidate branch ij is connected, and vice versa. Based on this method, the LSOCR-DOPF model in this paper needs to add the following constraints:

$$\begin{cases} P_{ij}^{\min} \sigma_{ij,t} \leq P_{ij,t} \leq P_{ij}^{\max} \sigma_{ij,t} \\ Q_{ij}^{\min} \sigma_{ij,t} \leq Q_{ij,t} \leq Q_{ij}^{\max} \sigma_{ij,t}, \forall ij \in E^{\text{SW}} \\ \bar{I}_{ij}^{\min} \sigma_{ij,t} \leq \bar{I}_{ij,t} \leq \bar{I}_{ij}^{\max} \sigma_{ij,t} \\ \sum_{ij \in E/E^{\text{SW}}} "1" + \sum_{ij \in E^{\text{SW}}} \sigma_{ij,t} = N^{\text{bus}} - N^{\text{sub}} \end{cases} \quad (33)$$

Equation (33) imposes a stringent restriction on the branch power flow. It serves as both necessary and sufficient conditions, which guarantee a certain level of load power balance. In a purely load-based grid, these conditions can ensure stability. However, in an active distribution network integrating DERs, there may arise the possibility of ring networks or isolated islands. The introduction of connectivity constraints can effectively eliminate such isolated island operations in the power grid. This can be achieved by setting the injection power of all non-substation nodes in the network to a small normal value ε and incorporating it into the power flow constraint, ensuring connectivity between each node and the substation node. The corresponding auxiliary equation is as follows:

$$\begin{cases} p_{j,t}^* = \sum_{k \in \delta(j)} P_{jk,t}^* - \sum_{i \in \pi(j)} \left(P_{ij,t}^* - \bar{I}_{ij,t}^* r_{ij} \right) + g_j \bar{V}_{j,t}^* = \varepsilon \\ q_{j,t}^* = \sum_{k \in \delta(j)} Q_{jk,t}^* - \sum_{i \in \pi(j)} \left(Q_{ij,t}^* - \bar{I}_{ij,t}^* x_{ij} \right) + b_j \bar{V}_{j,t}^* = \varepsilon \\ \bar{V}_{j,t}^* = \bar{V}_{j,t} - 2 \left(P_{ij,t}^* r_{ij} + Q_{ij,t}^* x_{ij} \right) + \bar{I}_{ij,t}^* \left(r_{ij}^2 + x_{ij}^2 \right), \forall j \in B, \forall ij \in E \end{cases} \quad (34)$$

So far, equations (33) and (34) ensure the radiation and connectivity in the network. At the same time, in the process of power grid reconstruction, the number of switch adjustments is also limited. Similar to the constraint on the number of OLTC adjustments in Section 2.2.1, the switch adjustment limit is modeled as follows:

$$\begin{cases} \delta_{ij,t}^{\text{SW,IN}} + \delta_{ij,t}^{\text{SW,DE}} \leq 1 \\ \sigma_{ij,t} - \sigma_{ij,t-1} \geq \delta_{ij,t}^{\text{SW,IN}} - \delta_{ij,t}^{\text{SW,DE}}, \forall t, \forall ij \in E^{\text{SW}} \\ \sigma_{ij,t} - \sigma_{ij,t-1} \leq \delta_{ij,t}^{\text{SW,IN}} - \delta_{ij,t}^{\text{SW,DE}} \end{cases} \quad (35)$$

where, $\delta_{ij,t}^{\text{sw,I}}$ and $\delta_{ij,t}^{\text{sw,DE}}$ represent the branch switch change identification, which is 0-1 variable, if $\delta_{ij,t}^{\text{sw,IN}} = 1$, then the switch changes from open state to closed state at time t , $\delta_{ij,t}^{\text{sw,DE}}$ can be obtained in the same way; $N_{ij}^{\text{sw,max}}$ is the maximum allowable adjustment times of the switch at time T .

2.2.3 ZIP load application

It is evident that the traditional approach of considering only constant power loads in demand is no longer adequate in the era of advanced technology and growing demand for refined simulation. Thus, it is imperative to develop a ZIP load modeling that accounts

for voltage static characteristics. As noted in [25], the load can be modeled using the ZIP model, which is comprised of constant power, constant current, and constant impedance models. For ease of expression, the time marker t has been omitted.

$$\begin{cases} P_j^{\text{Load}} = P_{j,0}^{\text{load}} \left(\alpha_j^A \frac{V_j^2}{V_{j,0}^2} + \alpha_j^B \frac{V_j}{V_{j,0}} + \alpha_j^C \right) \\ Q_j^{\text{Load}} = Q_{j,0}^{\text{load}} \left(\alpha_j^A \frac{V_j^2}{V_{j,0}^2} + \alpha_j^B \frac{V_j}{V_{j,0}} + \alpha_j^C \right) \end{cases} \quad (36)$$

where, α_j^A , α_j^B and α_j^C are the proportion of constant impedance load, constant current load and constant power load; $P_{j,0}^{\text{load}}$, $Q_{j,0}^{\text{load}}$ are the power demand under the rated voltage; According to the second-order cone relaxation principle, the model is equivalent to:

$$\begin{cases} P_j^{\text{Load}} = P_{j,0}^{\text{load}} \left(\alpha_j^A \frac{\bar{V}_j}{V_{j,0}} + \alpha_j^B \frac{\sqrt{\bar{V}_j}}{\sqrt{V_{j,0}}} + \alpha_j^C \right) \\ Q_j^{\text{Load}} = Q_{j,0}^{\text{load}} \left(\alpha_j^A \frac{\bar{V}_j}{V_{j,0}} + \alpha_j^B \frac{\sqrt{\bar{V}_j}}{\sqrt{V_{j,0}}} + \alpha_j^C \right) \end{cases} \quad (37)$$

where, for constant current load, $\sqrt{\bar{V}_j}$, since the unit value of voltage is near the rated voltage of 1.0, the square term is also near the rated value of 1.0, set $\bar{V}_j = 1 + \Delta\bar{V}_j$, $|\Delta\bar{V}_j| < 0.1$. By expanding it in Taylor series:

$$\sqrt{\bar{V}_j} = \sqrt{1 + \Delta\bar{V}_j} = 1 + \frac{1}{2} \Delta\bar{V}_j + o(\Delta\bar{V}_j^2) \quad (38)$$

It should be noted that:

$$\sqrt{\bar{V}_j} \approx 1 + \frac{1}{2} \Delta\bar{V}_j = \frac{1}{2} + \frac{1}{2} \bar{V}_j \quad (39)$$

$$\Psi(\bar{V}_j) = \left| \sqrt{\bar{V}_j} - \left(\frac{1}{2} + \frac{1}{2} \bar{V}_j \right) \right| \quad (40)$$

And the calculated equivalent error order is 10^{-3} , which fully meets the optimization requirements. Based on the above analysis, $\bar{V}_{j,0} = \sqrt{V_{j,0}} = 1$ is substituted into equation (37) to obtain:

$$\begin{cases} P_j^{\text{Load}} = \left(\alpha_j^A + \frac{\alpha_j^B}{2} \right) \bar{V}_j P_{j,0}^{\text{load}} + \left(\frac{\alpha_j^B}{2} + \alpha_j^C \right) P_{j,0}^{\text{load}} \\ Q_j^{\text{Load}} = \left(\alpha_j^A + \frac{\alpha_j^B}{2} \right) \bar{V}_j Q_{j,0}^{\text{load}} + \left(\frac{\alpha_j^B}{2} + \alpha_j^C \right) Q_{j,0}^{\text{load}} \end{cases} \quad (41)$$

2.3 Proposed LSOCR-DOPF optimization flowchart

The comprehensive optimization flowchart of LSOCR-DOPF is depicted in Figure 3. The comprehensive LSOCR-DOPF model described in this paper is comprised of the preliminary LSOCR-DOPF model (Equation 19) introduced in Section 2.1.3 and all of the linearized models outlined in Section 2.2. The LSOCR-DOPF is a classic Mixed Integer Linear Programming (MILP) problem, which can be modeled using the YALMIP toolkit in MATLAB and efficiently solved by invoking advanced solvers.



<div style="background-color: #008000; color: white; text-align: center; padding: 2px;">1</div> <div style="border: 1px solid black; padding: 2px; text-align: center;">Target</div>	<p>The network loss, main network power purchase cost and power abandonment</p> $C^{OPE} = \sum_{t \in T} \Delta t \left[\sum_{ij \in E} c^{Loss} \bar{I}_{ij,t} r_{ij} + \sum_{j \in B^{TR}} c^{TR} P_{j,t}^{TR} + \sum_{j \in B^{PVG}} c^{PVG} (P_{j,t}^{PVG} - P_{j,t}^{PVG,PRE}) + \sum_{j \in B^{WTG}} c^{WTG} (P_{j,t}^{WTG} - P_{j,t}^{WTG,PRE}) \right]$
<div style="background-color: #ff8c00; color: white; text-align: center; padding: 2px;">2</div> <div style="border: 1px solid black; padding: 2px; text-align: center;">S.t.</div>	<ul style="list-style-type: none"> ➤ Node injection power constraint; Eqs. (10),(11),(16) ➤ Node voltage constraint; Eq. (13) ➤ Branch current constraint; Eq. (14) ➤ polyhedral approximations constraints; Eq. (17) ➤ active management device; Eqs. (20)-(32) <li style="padding-left: 20px;">(OLTC, CB, SVC,ESS,DG,ZIP, etc.) ➤ Network reconfiguration constraints; Eq. (35) ➤ Radial topology constraints; Eq. (33) ➤ No island operation restriction; Eq. (34) ➤ ZIP load; Eq. (41)
<div style="background-color: #0000ff; color: white; text-align: center; padding: 2px;">3</div> <div style="border: 1px solid black; padding: 2px; text-align: center;">Cases</div>	
<div style="background-color: #800080; color: white; text-align: center; padding: 2px;">4</div> <div style="border: 1px solid black; padding: 2px; text-align: center;">Solver</div>	

Figure 3. Proposed LSOCR-DOPF optimization flowchart.

3 Validation and discussions

This paper mainly analyzes the application of three scenarios based on LSOCR-DOPF: 1) Power coordination optimization; 2) Network reconstruction; 3) ZIP load application. The numerical simulation analysis was carried out using an active distribution system based on the IEEE33 and IEEE69 bus system data. The simulation parameters of the basic simulation system are presented in the Appendix. The simulation was performed on a 64-bit Windows 11 operating system with an Intel(R) Core (TM) i7-6700HQ CPU @ 2.64GHz and 24 GB RAM, using MATLAB R2022b and calling YALMIP and GUROBI 10.0. The dynamic simulation period was set to 24 hours.

3.1 Power coordination optimization

3.1.1 scenario description

This scenario (Figure 4) adds elements such as OLTC, ESS, CB, SVC, Wind and photovoltaic (PV) to the basic IEEE33 network to comprehensively verify the application effect of each active management object in LSOCR-DOPF. Assuming the OLTC transformation ratio range is 1 - 6%.

The validity of the similar relaxation model has been demonstrated in Refs. [14,17]. To further verify its universality, this scenario incorporates the cost of power purchase from the main network, as well as penalty costs for the abandonment of wind and photovoltaic power. The resulting total operational cost (C^{OPE}) is as follows:

$$C^{OPE} = \sum_{t \in T} \Delta t \left[\sum_{ij \in E} c^{Loss} \bar{I}_{ij,t} r_{ij} + \sum_{j \in B^{TR}} c^{TR} P_{j,t}^{TR} + \sum_{j \in B^{PVG}} c^{PVG} (P_{j,t}^{PVG} - P_{j,t}^{PVG,PRE}) + \sum_{j \in B^{WTG}} c^{WTG} (P_{j,t}^{WTG} - P_{j,t}^{WTG,PRE}) \right] \quad (42)$$

where, c^{Loss} , c^{TR} , c^{WTG} and c^{PVG} are respectively the network loss price, the main network power purchase price, the wind power abandonment price and the photovoltaic power abandonment penalty price; $P_{j,t}^{PVG}$ and $P_{j,t}^{WTG}$ is the predicted output of wind power and photovoltaic respectively.

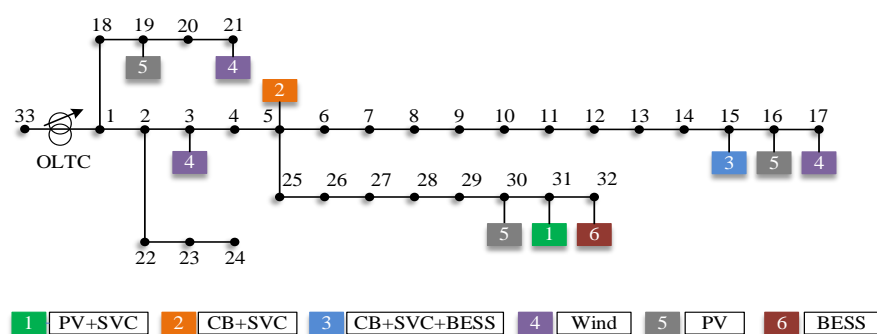


Figure 4. IEEE33 test active distribution network.

3.1.2 Analysis of optimization results

The multi-period operational results of the power coordination and optimization of each active management unit are obtained based on the original data of the scenario, as depicted in Figs. 5-10. Figs. 5-9 show the active load demand, the active output of each wind turbine unit, the PV active output, the active output of the main grid and the node injection power respectively, and the active power of energy storage charging and discharging. Figure 10 presents the total of 24 hours CB reactive power output and SVC reactive power output.

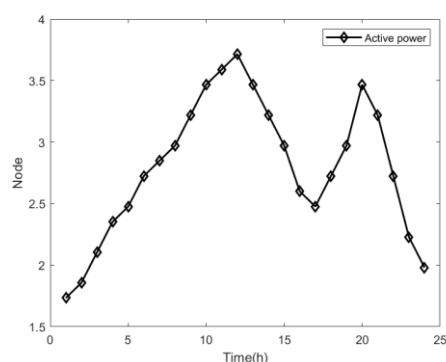


Figure 5. 24-hour active load diagram.

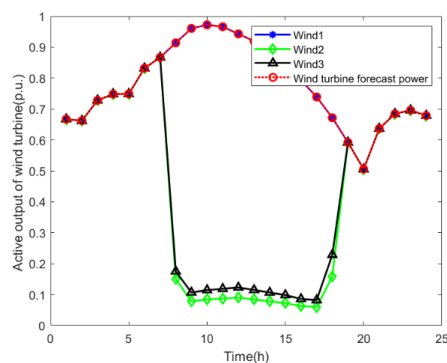


Figure 6. 24-hour wind turbine output diagram.

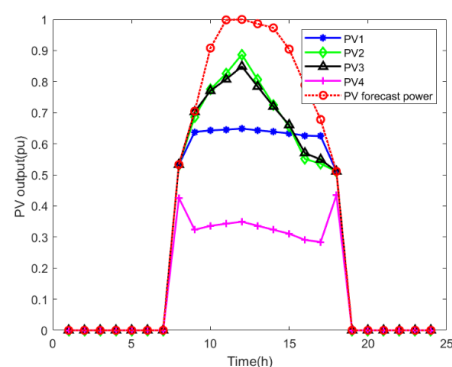


Figure 7. 24-hour PV output diagram.

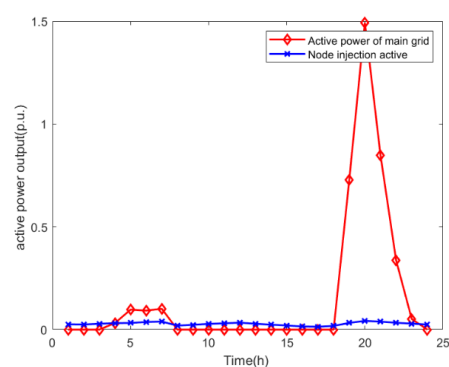


Figure 8. Active power output of main power grid and active power diagram of node injection in 24 hours.

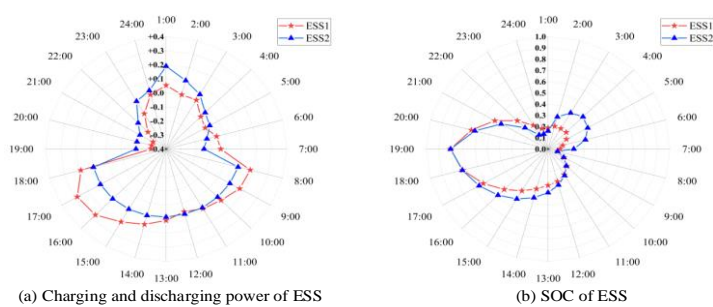


Figure 9. SOC and charging and discharging of ESS .

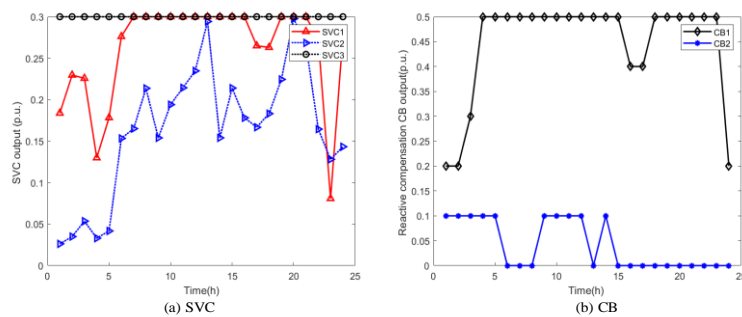


Figure 10. 24-hour Reactive compensation power (SVC+CB) diagram.

It can be seen from Figs. 5-10 that:

1) During the peak load periods (08:00-15:00, 19:00-21:00), the active load demand of the system can be met while the Energy Storage System (ESS) is unable to absorb the surplus clean energy due to its own charging limitations, resulting in power abandonment. The ESS discharges during both the peak load period and the low peak period of renewable energy generation, effectively reducing the peak-valley difference of the equivalent load;

2) During periods when the proportion of renewable energy output to load is relatively high (6:00-15:00, 18:00-22:00), reactive power compensation devices (Static Var Compensators (SVC) and Capacitor Banks (CB)) absorb the excess reactive power of the system, avoiding overvoltage.

Hence, the LSOCR-DOPF model proposed in this paper demonstrates significant effects on the optimization of both active and reactive power.

3.1.3 Model validity analysis

The LSOCR-DOPF is analyzed under three situations: "relaxation accuracy, calculation efficiency, and comparison of different optimization cases".

1) Relaxation accuracy

The relaxation accuracy of the objective function such as network loss has been proved and verified in the pure load network environment. However, considering the further analysis of the model accuracy after increasing the main network output, power abandonment, and load loss penalty costs, it is necessary to define the error index: $\Delta_{ij,t}^{\text{diff}} = |P_{ij,t}^2 + Q_{ij,t}^2 - \bar{I}_{i,t} \bar{U}_{j,t}|$.

Figure 11 shows the error scatter diagram of each branch in one day. Obviously, the deviation after relaxation meets the requirements of accurate operation, which is 10^{-6} .

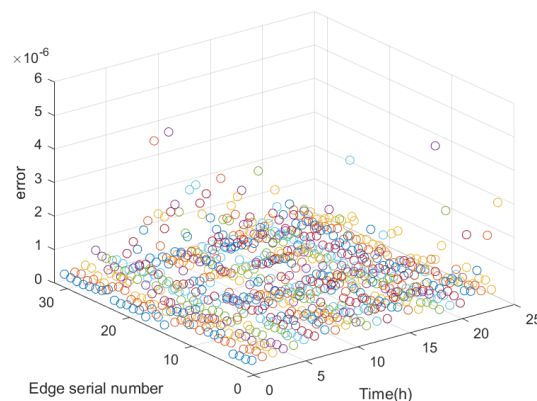


Figure 11. Scatter chart of error under each branch in each period.

2) Calculation timeliness

Table 1 presents the solution speed and respective simulation results under various objective functions. Specifically, The objective functions of each simulated operating conditions are as follows: Case 1: minimized network loss; Case 2: minimized power purchase cost of the main grid; Case 3: minimum power loss; Case 4: minimized network loss and main grid power purchase cost; Case 5: minimized network loss, main grid power purchase cost, and power abandonment. Table 1 shows the solution speed and corresponding simulation results under different objective functions. Among them, the objective function Case1 of each simulated operation condition is the minimum network loss; Case2: the minimum power purchase cost of the main network; Case3: Minimal power loss; Case4: network loss and main network power purchase cost are the least; Case 5: The network loss, main network power purchase cost and power abandonment are the minimum.

Table 1 Optimization results under four types of objective functions.

Case	Time (s)	Target (10^3 \$)		
		Network loss	Power purchase cost	Power abandonment
1	20.394	0.244	10.937	22.939
2	18.581	3.274	1.890	10.728
3	8.555	10.013	4.757	6.752
4	125.044	0.337	1.890	13.673
5	200.482	4.796	1.890	9.087

Based on Table 1, with the increase of the objective function, the calculation time continues to increase, but the calculation speed is still acceptable, the maximum is 200s, which meets the time requirements for day-ahead dispatching and real-time optimization of the active operation in the active distribution network.

Further, based on Case 1, this part compares the solving efficiency of MINLP (Interior Point-DOPF, Mixed-Integer Nonlinear Programming) model, MISOCP (SOCR-DOPF) model and MILP (LSOCR-DOPF) model of DOPF problem, and the results are summarized in Table 2. It can be seen from Table 2 that the accuracy and efficiency of LSOCP and SOCR are higher than those of the traditional interior point method. The distribution network loss optimization result of the MILP model linearized by SOCR is equal to the result of the MISOCP model, but the solution speed has been improved to a certain extent. This fully shows that the optimization efficiency can be improved by the LSOCP, which can reach 25%~30% (compared with SOCR). It is shown that the LSOCP method is slightly better than the SOCR method in terms of comprehensive solution efficiency, but its solution timeliness is completely better than the traditional interior point method.

Table 2 Comparison of optimization results of DOPF.

Net-work	Target (10^3 \$)			Time (s)		
	MINLP	MISOCP	MILP	MINLP	MISOCP	MILP
IEEE33	0.352	0.244	0.244	>5h	20.394	14.564
IEEE69	1.556	1.356	1.356	>5h	27.396	20.509

3) Comparison among different optimization cases

According to Tables 1-2, it can be seen that:

① In Case 1, only the optimization of network loss is considered, leading to substantial waste of clean energy power. On the other hand, Case 2 prioritizes the minimization of main grid power purchase costs, which results in increased consumption of clean energy, reducing the main grid power purchase and, in turn, reducing power waste. Conversely, Case 3 focuses on minimizing power loss. In comparison to Case 1, it requires more utilization of clean energy to reduce main grid power purchases, but results in an increase in network loss;

② In Case 4, the objective is to simultaneously minimize both the network loss and the main network's power purchase. The results show that while the main network's power purchase remains unchanged, the network loss decreases, but the amount of power abandonment increases. The paper assumes that the cost of network loss and the penalty cost of power abandonment are both equal to 5000 \$/MWh, which suggests that excessive access to clean energy may increase the network loss of the system;

③ Case 5 aims to minimize the network loss, main network power purchase and power abandonment. The main network power purchase remains the same, while the power abandonment decreases correspondingly, and the network loss increases, which means that the network loss caused by increasing the access to clean energy is less than

the penalty of clean energy power abandonment, so the power abandonment is further reduced.

④ To assess the impact of the active management equipment (SVC, CB, ESS) introduced in this paper on the performance of the distribution network, three tests were designed and included: (a) No addition of energy storage and reactive power compensation equipment; (b) Addition of an energy storage device in place of a reactive compensation device; (c) Simultaneous addition of both an energy storage device and a reactive compensation device. It can be seen from Figure 12 that adding the active management unit can improve the uniform distribution of voltage in the distribution network to some extent, which shows some functions of the active management unit. It is worth mentioning that the relatively elevated node voltage depicted in Figure 12 can be attributed to the network loss specified by the objective function.

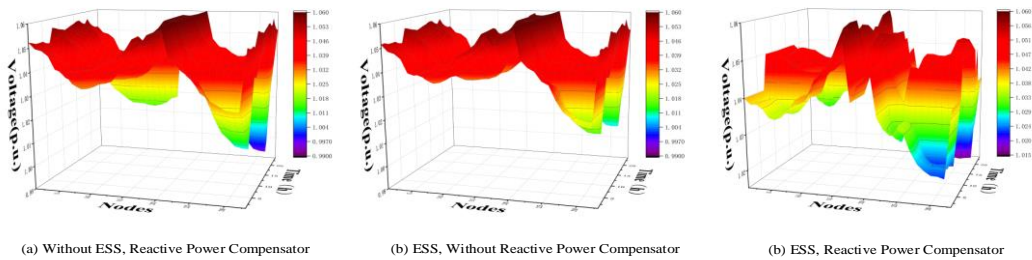


Figure 12. Voltage of different nodes (comparative verification).

3.2 Network reconfiguration

The distribution network reconfiguration scenario is analyzed based on the standard IEEE 33 systems (Appendix), and the load value is the original system data. In order to verify the effectiveness of second-order cone relaxation in distribution network reconstruction, this example uses static single-period reconstruction for analysis. In the two examples, node 1 is a substation node with voltage amplitude of 1.06pu. It is assumed that each branch is equipped with section switch, and the optimization calculation is carried out with the goal of minimizing the network loss. The results are shown in Table 3. Also solve the error scatter diagram of each branch, as shown in Figure 13.

Table 3 Reconfiguration scheme and optimization results.

IEEE33	Time(s)	Network loss (MW)	Original network loss (MW)	Disconnected switch
Single-period	1.355014	0.0256	0.0368	7(6-7), 9(8-9), 14(13-14), 32(31-32),
Multi-period	153.404963	1.7080	2.4964	37(24-28)

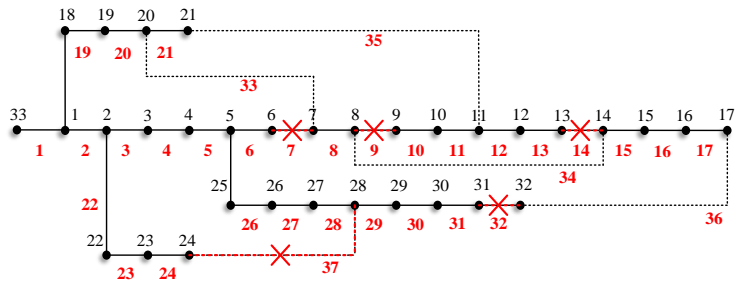


Figure 13. Optimized and reconstructed IEEE33 network (Node serial number is given by black numbers, branch serial number is shown by red numbers, and red cross and red dotted line indicate disconnected branch).

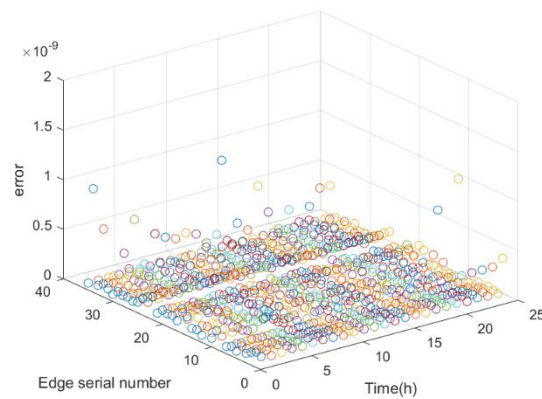


Figure 14. Scatter diagram of distribution network reconfiguration error.

As shown in Figure 14, It is not difficult to find that the error is 10^{-9} orders of magnitude, meeting the reconstruction requirements. It is worth noting that in this example, no active management equipment is added. For IEEE 33 nodes, all nodes have load values, so only equation (33) can be added to the radiation constraint. For some nodes in the IEEE69 system without load, equation (34) must be added to ensure that all nodes are connected and operate without islands and radiation.

3.3 ZIP load application

This scenario adopts PG69 node system test (Figure 15). In order test the static voltage characteristics of the load, this part does not consider the active management unit, and only analyzes the calculation results after citing the static voltage characteristics of the load. Three types of loads, namely constant power, constant current and constant impedance, are added to each node. The voltage distribution of each node at each time is calculated as shown in Figure 16. Figure 17 shows the comparison of load active demand considering voltage static characteristics or not.

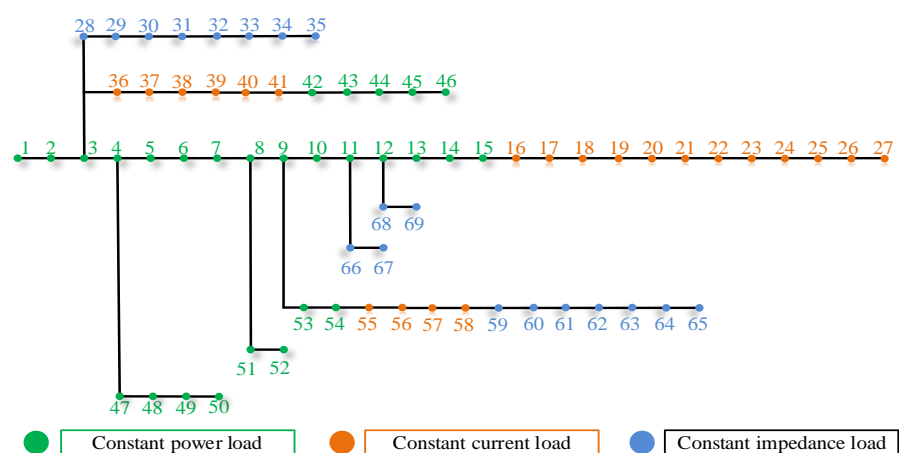


Figure 15. IEEE69 test active distribution network.

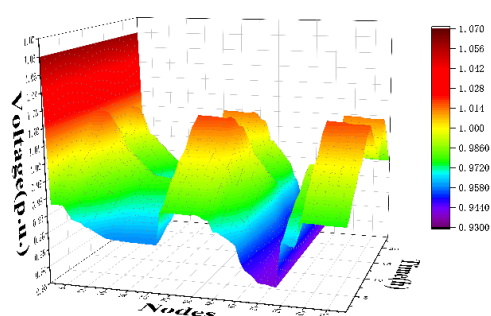


Figure 16. Voltage distribution diagram of each node.

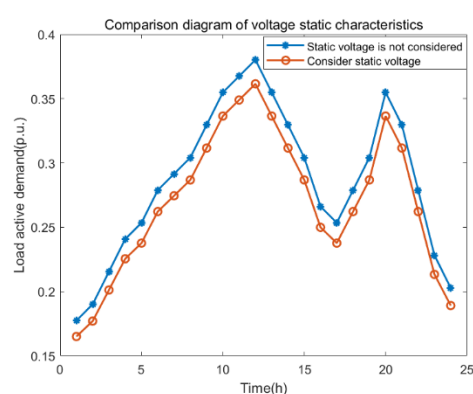


Figure 17. Comparison of load active demand considering voltage static characteristics or not.

As can be seen from Figure 16 and Figure 17, since most of the node voltage is lower than 1.0pu, the load demand will be reduced after considering the static voltage characteristics of the load. It is important to consider the static voltage characteristics of active distribution network fine simulation. In addition, the second-order cone relaxation error of each period is shown in Figure 18. Obviously, the relaxation effect is also very satisfactory.

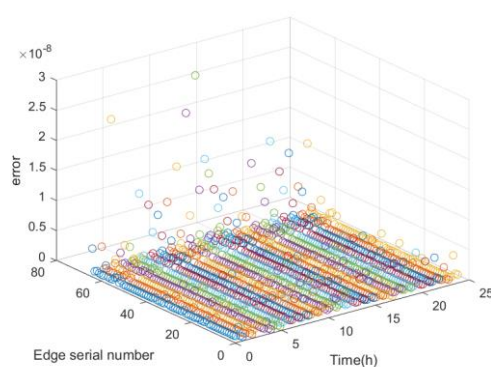


Figure 18. Error scatter chart of ZIP load model.

4. Conclusions

In this paper, a polyhedral linear approximation method of the second-order cone relaxation (LSOCR-DOPF) for the dynamic optimal power flow problem based on the

branch power flow model of the distribution network is proposed and validated. Detailed linear constraint modeling of active management units is performed, and the effectiveness of the proposed solution method is verified through comparison with other solutions in three major application scenarios. The results demonstrate that LSOCR-DOPF meets the requirements of timely calculation and accuracy in the fields of day-ahead optimal dispatch, real-time operation, and efficient control for active distribution networks. Additionally, the results highlight the importance of accurately modeling ZIP load in active distribution networks. Further, the inclusion of discrete variables, which are non-convex sources, has an impact on the accuracy of the relaxation model, and the universality condition of the second-order cone relaxation model requires further theoretical investigation.

Supplementary Materials: Not applicable.

Author Contributions: Conceptualization, W. M and X.D; methodology, W. M; software, W. M; validation, W. M and J.Y; formal analysis, W. M and R.M.R.-A.; investigation, M. D; resources, W. M; data curation, W. M and X. D; writing—original draft preparation, X.D. and W. M; writing—review and editing, V.S.; visualization, W. M; supervision, D.S; project administration, X.D.; funding acquisition, X.D. All authors have read and agreed to the published version of the manuscript.

Funding: This research was supported by National natural science foundation of China under Grant 62211540397 and an internal grant project of VSB-Technical University of Ostrava (SGS project, grant number SP2022/77).

Data Availability Statement: Not applicable.

Acknowledgments: Not applicable.

Conflicts of Interest: The authors declare no conflict of interest.

Appendix A

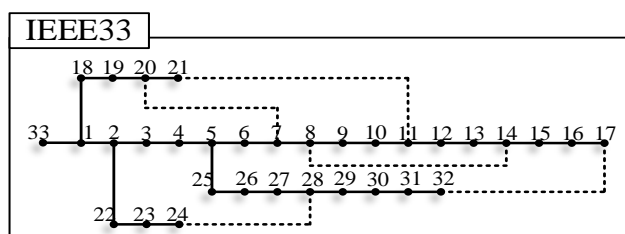


Figure 1 IEEE33 Radial Distribution Network.

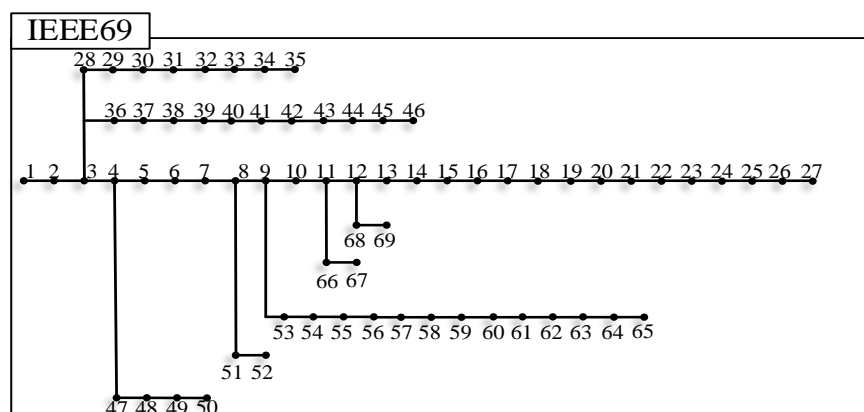


Figure 2 IEEE69 Radial Distribution Network.

Table 1: System data for 69-bus radial distribution network (“*” denotes a tie-line).

Branch Number	Sending Bus	Receiving Bus	Resistance Ω	Reactance Ω	Nominal Load at Receiving Bus		Maximum Line Capacity (kVA)
					P (kW)	Q(kVA)	
1	1	2	0.0005	0.0012	0.0	0.0	10761
2	2	3	0.0005	0.0012	0.0	0.0	10761
3	3	4	0.0015	0.0036	0.0	0.0	10761
4	4	5	0.0251	0.0294	0.0	0.0	5823
5	5	6	0.3660	0.1864	2.60	2.20	1899
6	6	7	0.3811	0.1941	40.40	30.00	1899
7	7	8	0.0922	0.0470	75.00	54.00	1899
8	8	9	0.0493	0.0251	30.00	22.00	1899
9	9	10	0.8190	0.2707	28.00	19.00	1455
10	10	11	0.1872	0.0619	145.00	104.00	1455
11	11	12	0.7114	0.2351	145.00	104.00	1455
12	12	13	1.0300	0.3400	8.00	5.00	1455
13	13	14	1.0440	0.3450	8.00	5.50	1455
14	14	15	1.0580	0.3496	0.0	0.0	1455
15	15	16	0.1966	0.0650	45.50	30.00	1455
16	16	17	0.3744	0.1238	60.00	35.00	1455
17	17	18	0.0047	0.0016	60.00	35.00	2200
18	18	19	0.3276	0.1083	0.0	0.0	1455

19	19	20	0.2106	0.0690	1.00	0.60	1455
20	20	21	0.3416	0.1129	114.00	81.00	1455
21	21	22	0.0140	0.0046	5.00	3.50	1455
22	22	23	0.1591	0.0526	0.0	0.0	1455
23	23	24	0.3463	0.1145	28.00	20.0	1455
24	24	25	0.7488	0.2475	0.0	0.0	1455
25	25	26	0.3089	0.1021	14.0	10.0	1455
26	26	27	0.1732	0.0572	14.0	10.0	1455
27	3	28	0.0044	0.0108	26.0	18.6	10761
28	28	29	0.0640	0.1565	26.0	18.6	10761
29	29	30	0.3978	0.1315	0.0	0.0	1455
30	30	31	0.0702	0.0232	0.0	0.0	1455
31	31	32	0.3510	0.1160	0.0	0.0	1455
32	32	33	0.8390	0.2816	14.0	10.0	2200
33	33	34	1.7080	0.5646	9.50	14.00	1455
34	34	35	1.4740	0.4873	6.00	4.00	1455
35	3	36	0.0044	0.0108	26.0	18.55	10761
36	36	37	0.0640	0.1565	26.0	18.55	10761
37	37	38	0.1053	0.1230	0.0	0.0	5823
38	38	39	0.0304	0.0355	24.0	17.00	5823
39	39	40	0.0018	0.0021	24.0	17.00	5823
40	40	41	0.7283	0.8509	1.20	1.0	5823
41	41	42	0.3100	0.3623	0.0	0.0	5823
42	42	43	0.0410	0.0478	6.0	4.30	5823
43	43	44	0.0092	0.0116	0.0	0.0	5823
44	44	45	0.1089	0.1373	39.22	26.30	5823
45	45	46	0.0009	0.0012	39.22	26.30	6709
46	4	47	0.0034	0.0084	0.00	0.0	10761
47	47	48	0.0851	0.2083	79.00	56.40	10761
48	48	49	0.2898	0.7091	384.70	274.50	10761
49	49	50	0.0822	0.2011	384.70	274.50	10761
50	8	51	0.0928	0.0473	40.50	28.30	1899
51	51	52	0.3319	0.1114	3.60	2.70	2200

52	52	53	0.1740	0.0886	4.35	3.50	1899
53	53	54	0.2030	0.1034	26.40	19.00	1899
54	54	55	0.2842	0.1447	24.00	17.20	1899
55	55	56	0.2813	0.1433	0.0	0.0	1899
56	56	57	1.5900	0.5337	0.0	0.0	2200
57	57	58	0.7837	0.2630	0.0	0.0	2200
58	58	59	0.3042	0.1006	100.0	72.0	1455
59	59	60	0.3861	0.1172	0.0	0.0	1455
60	60	61	0.5075	0.2585	1244.0	888.00	1899
61	61	62	0.0974	0.0496	32.0	23.00	1899
62	62	63	0.1450	0.0738	0.0	0.0	1899
63	63	64	0.7105	0.3619	227.0	162.00	1899
64	64	65	1.0410	0.5302	59.0	42.0	1899
65	11	66	0.2012	0.0611	18.0	13.0	1455
66	66	67	0.0047	0.0014	18.0	13.0	1455
67	12	68	0.7394	0.2444	28.0	20.0	1455
68	68	69	0.0047	0.0016	28.0	20.0	1455
69*	11	43	0.5000	0.5000			566
70*	13	21	0.5	0.5			566
71*	15	46	1.0	1.0			400
72*	50	59	2.0	2.0			283
73*	27	65	1.0	1.0			400

Table 2: System data for 33-bus radial distribution network.

624

Branch Number	Sending Bus	Receiving Bus	Resistance Ω	Reactance Ω	Nominal Load at Receiving Bus	
					P (kW)	Q (kVA)
1	1	2	0.0922	0.047	100	60
2	2	3	0.493	0.2511	90	40
3	3	4	0.366	0.1864	120	80
4	4	5	0.3811	0.1941	60	30
5	5	6	0.819	0.707	60	20
6	6	7	0.1872	0.6188	200	100
7	7	8	0.7114	0.2351	200	100
8	8	9	1.03	0.74	60	20
9	9	10	1.044	0.74	60	20

10	10	11	0.1966	0.065	45	30
11	11	12	0.3744	0.1298	60	35
12	12	13	1.468	1.155	60	35
13	13	14	0.5416	0.7129	120	80
14	14	15	0.591	0.526	60	10
15	15	16	0.7463	0.545	60	20
16	16	17	1.289	1.721	60	20
17	17	18	0.732	0.574	90	40
18	2	19	0.164	0.1565	90	40
19	19	20	1.5042	1.3554	90	40
20	20	21	0.4095	0.4784	90	40
21	21	22	0.7089	0.9373	90	40
22	3	23	0.4512	0.3083	90	50
23	23	24	0.898	0.7091	420	200
24	24	25	0.896	0.7011	420	200
25	6	26	0.203	0.1034	60	25
26	26	27	0.2842	0.1447	60	25
27	27	28	1.059	0.9337	60	20
28	28	29	0.8042	0.7006	120	70
29	29	30	0.5075	0.2585	200	600
30	30	31	0.9744	0.963	150	70
31	31	32	0.3105	0.3619	210	100
32	32	33	0.341	0.5302	60	40
33	20	7	2.0000	2.0000	-	-
34	8	14	2.0000	2.0000	-	-
35	11	21	2.0000	2.0000	-	-
36	17	32	0.5000	0.5000	-	-
37	24	28	0.5000	0.5000	-	-

References

1. Davarzani, S.; Pisica, I.; Taylor, G.A.; Munisami, K.J. Residential Demand Response Strategies and Applications in Active Distribution Network Management. *Renewable and Sustainable Energy Reviews* **2021**, *138*, 110567, doi:<https://doi.org/10.1016/j.rser.2020.110567>.
2. Kryonidis, G.C.; Kontis, E.O.; Papadopoulos, T.A.; Pippi, K.D.; Nousedilis, A.I.; Barzegkar-Ntovom, G.A.; Boubaris, A.D.; Papanikolaou, N.P. Ancillary services in active distribution networks: A review of technological trends from operational and online analysis perspective. *Renewable and Sustainable Energy Reviews* **2021**, *147*, 111198, doi:<https://doi.org/10.1016/j.rser.2021.111198>.
3. Liu, J.; Song, D.; Li, Q.; Yang, J.; Hu, Y.; Fang, F.; Joo, Y.H. Life cycle cost modelling and economic analysis of wind power: A state of art review. *Energy Conversion and Management* **2023**, *277*, 116628.
4. Papadimitrakis, M.; Giamarellos, N.; Stogiannos, M.; Zois, E.N.; Livanos, N.A.I.; Alexandridis, A. Metaheuristic search in smart grid: A review with emphasis on planning, scheduling and power flow optimization applications. *Renewable and Sustainable Energy Reviews* **2021**, *145*, doi:10.1016/j.rser.2021.111072.
5. Song, D.; Meng, W.; Dong, M.; Yang, J.; Wang, J.; Chen, X.; Huang, L. A critical survey of integrated energy system: Summaries, methodologies and analysis. *Energy Conversion and Management* **2022**, *266*, 115863, doi:<https://doi.org/10.1016/j.enconman.2022.115863>.
6. Bienstock, D.; Verma, A. Strong NP-hardness of AC power flows feasibility. *Operations Research Letters* **2019**, *47*, 494–501.
7. Lehmann, K.; Grastien, A.; Van Hentenryck, P. AC-feasibility on tree networks is NP-hard. *IEEE Transactions on Power Systems*

- 2015, 31, 798–801. 642
8. Castillo, A.; O'Neill, R. Survey of Approaches to Solving the ACOPF: Optimal Power Flow Paper 4. *FERC Staff Technical Paper*. 2013, 1. 643
9. Stott, B.; Jardim, J.; Alsac, O. DC power flow revisited. *IEEE Transactions on Power Systems* **2009**, *24*, 1290–1300. 644
10. Taylor, J.A. *Convex optimization of power systems*; Cambridge University Press: 2015. 645
11. Makhadmeh, S.N.; Khader, A.T.; Al-Betar, M.A.; Naim, S.; Abasi, A.K.; Alyasseri, Z.A.A. Optimization methods for power scheduling problems in smart home: Survey. *Renewable and Sustainable Energy Reviews* **2019**, *115*, 109362. 646
12. Baker, K. Solutions of DC OPF are never AC feasible. In Proceedings of the Proceedings of the Twelfth ACM International Conference on Future Energy Systems, 2021; pp. 264–268. 647
13. Farivar, M.; Low, S.H. Branch Flow Model: Relaxations and Convexification-Part II. *Ieee Transactions on Power Systems* **2013**, *28*, 2565–2572, doi:10.1109/tpwrs.2013.2255318. 648
14. Farivar, M.; Low, S.H. Branch flow model: Relaxations and convexification—Part I. *IEEE Transactions on Power Systems* **2013**, *28*, 2554–2564. 649
15. Baran, M.E.; Wu, F.F. Network reconfiguration in distribution systems for loss reduction and load balancing. *IEEE Transactions on Power delivery* **1989**, *4*, 1401–1407. 650
16. Low, S.H. Convex relaxation of optimal power flow—Part I: Formulations and equivalence. *IEEE Transactions on Control of Network Systems* **2014**, *1*, 15–27. 651
17. Low, S.H. Convex relaxation of optimal power flow—Part II: Exactness. *IEEE Transactions on Control of Network Systems* **2014**, *1*, 177–189. 652
18. Gan, L.; Li, N.; Topcu, U.; Low, S.H. Exact convex relaxation of optimal power flow in radial networks. *IEEE Transactions on Automatic Control* **2014**, *60*, 72–87. 653
19. Nick, M.; Cherkaoui, R.; Le Boudec, J.-Y.; Paolone, M. An exact convex formulation of the optimal power flow in radial distribution networks including transverse components. *IEEE Transactions on Automatic Control* **2017**, *63*, 682–697. 654
20. Christakou, K.; Tomozei, D.-C.; Le Boudec, J.-Y.; Paolone, M. AC OPF in radial distribution networks—Part I: On the limits of the branch flow convexification and the alternating direction method of multipliers. *Electric Power Systems Research* **2017**, *143*, 438–450. 655
21. Ben-Tal, A.; Nemirovski, A. On polyhedral approximations of the second-order cone. *Mathematics of Operations Research* **2001**, *26*, 193–205. 656
22. Kocuk, B. Rational polyhedral outer-approximations of the second-order cone. *Discrete Optimization* **2021**, *40*, 100643. 657
23. Ferreira, R.S.; Borges, C.L.T.; Pereira, M.V. A flexible mixed-integer linear programming approach to the AC optimal power flow in distribution systems. *IEEE Transactions on Power Systems* **2014**, *29*, 2447–2459. 658
24. Zografou-Barredo, N.-M.; Patsios, C.; Sarantakos, I.; Davison, P.; Walker, S.L.; Taylor, P.C. MicroGrid resilience-oriented scheduling: A robust MISOCP model. *IEEE Transactions on Smart Grid* **2020**, *12*, 1867–1879. 659
25. Garces, A. A quadratic approximation for the optimal power flow in power distribution systems. *Electric Power Systems Research* **2016**, *130*, 222–229, doi:<https://doi.org/10.1016/j.epsr.2015.09.006>. 660
26. Fathi, R.; Tousi, B.; Galvani, S. Allocation of renewable resources with radial distribution network reconfiguration using improved salp swarm algorithm. *APPLIED SOFT COMPUTING* **2023**, *132*, doi:10.1016/j.asoc.2022.109828. 661
27. Ding, T.; Liu, S.; Yuan, W.; Bie, Z.; Zeng, B. A two-stage robust reactive power optimization considering uncertain wind power integration in active distribution networks. *IEEE Transactions on Sustainable Energy* **2015**, *7*, 301–311. 662
28. Song, D.; Yan, J.; Zeng, H.; Deng, X.; Yang, J.; Qu, X.; Rizk-Allah, R.M.; Snášel, V.; Joo, Y.H. Topological Optimization of an Offshore-Wind-Farm Power Collection System Based on a Hybrid Optimization Methodology. *Journal of Marine Science and Engineering* **2023**, *11*, 279. 663
29. Ehsan, A.; Yang, Q. State-of-the-art techniques for modelling of uncertainties in active distribution network planning: A review. *Applied Energy* **2019**, *239*, 1509–1523, doi:<https://doi.org/10.1016/j.apenergy.2019.01.211>. 664
30. Mishra, D.K.; Ghadi, M.J.; Azizivahed, A.; Li, L.; Zhang, J. A review on resilience studies in active distribution systems. *Renewable and Sustainable Energy Reviews* **2021**, *135*, 110201, doi:<https://doi.org/10.1016/j.rser.2020.110201>. 665
31. He, L.; Yang, J.; Yan, J.; Tang, Y.; He, H. A bi-layer optimization based temporal and spatial scheduling for large-scale electric vehicles. *Applied energy* **2016**, *168*, 179–192. 666
32. Xiang, Y.; Liu, J.; Liu, Y. Optimal active distribution system management considering aggregated plug-in electric vehicles. *Electric Power Systems Research* **2016**, *131*, 105–115. 667

Disclaimer/Publisher's Note: The statements, opinions and data contained in all publications are solely those of the individual author(s) and contributor(s) and not of MDPI and/or the editor(s). MDPI and/or the editor(s) disclaim responsibility for any injury to people or property resulting from any ideas, methods, instructions or products referred to in the content.

698

699